Electronic structure and chemical bonding in PuO_2

Yu. A. Teterin,* K. I. Maslakov,† A. Yu. Teterin, and K. E. Ivanov
NRC Kurchatov Institute, Moscow, 123182, Russia

M. V. Ryzhkov
Ural Department of RAS, Institute of Solid State Chemistry, Ekaterinburg, 620990 Russia

V. G. Petrov, D. A. Enina, and St. N. Kalmykov
Radiochemistry Division, Chemistry Department, Lomonosov Moscow State University, Moscow, 119991 Russia
(Received 6 February 2013; revised manuscript received 22 April 2013; published 12 June 2013)

Quantitative analysis of the x-ray photoelectron spectra structure in the binding energy (BE) range of 0 eV–∼35 eV for plutonium dioxide (PuO_2) valence electrons was done. The BEs and structure of the core electronic shells (35 eV–1250 eV BE), as well as the relativistic discrete variation calculation results for the finite fragments of the PuO_2 lattice and the data of other authors, were taken into account. The experimental data show that the many-body effects and the multiplet splitting contribute to the spectral structure much less than the outer (0 eV–∼15 eV) and the inner (∼15 eV–∼35 eV) valence molecular orbitals (OVMO and IVMO, respectively). The filled Pu $5f$ electronic states were shown to form in the PuO_2 valence band. The Pu $6p$ electrons participate in the formation of both the IVMO and the OVMO (bands). The filled Pu $6p_{3/2}$ and the O $2s$ electronic shells were found to take maximum part in the IVMO formation. The MO composition and the sequence order in the BE range of 0 eV–∼35 eV in PuO_2 were established. The experimental and theoretical data allowed a quantitative MO scheme for PuO_2, which is fundamental for understanding both the chemical bond nature in plutonium dioxide and the interpretation of other x-ray spectra of PuO_2.

DOI: 10.1103/PhysRevB.87.245108 PACS number(s): 71.20.Gj, 82.80.Ej, 33.60.+q, 61.50.Lt

I. INTRODUCTION

The study of the plutonium electronic structure and the chemical bond nature in plutonium compounds is a topic of great interest.[1–3] Thus, the photoelectron spectra structure of plutonium and plutonium oxides (PuO_x) in the outer valence band binding energy (BE) range of 0 eV–∼15 eV was studied.[4–9] The x-ray photoelectron spectra (XPS),[2,8,10–17] as well as the spectra of electron energy loss and the absorption spectra[14,18] of metallic plutonium, the XPS of oxides,[19–28] and the resonant photoemission spectra of Pu (Refs. 8, 29, and 30) were studied. When studying the XPS of plutonium and its oxides (PuO_x), most authors, except for the authors of Refs. 10, 19, 20, and 22, paid special attention to the outer valence electron BE range (0 eV–∼15 eV) and the core Pu $4f$ shell. The Pu $4f$ XPS structure is typical for metallic Pu and its oxides and can be used for identification of Pu oxidation states. However, the core shell Pu $4p, 4d, 5s, 5p, 5d$, and $6s$ structures were not well studied.[20] The absence of the experimental XPS of these core shells for PuO_2 did not allow an interpretation of the fine XPS structure using the theoretical calculation data. Also the XPS structure of the inner valence shells in PuO_2 in the BE range of ∼15 eV–∼35 eV was studied only on the qualitative level.[22]

The XPS study of the electronic structure of compounds,[31] which includes lanthanides[32] and actinides,[33] their oxidation states, physical and chemical properties, and chemical bond nature, in addition to their chemical shifts (ΔE_b) and peak intensities (I_0), can use the core and valence spectral structure parameters. This spectral structure can originate from the formation of the outer (0 eV–∼15 eV) and the inner (∼15–∼35 eV) valence molecular orbitals (OVMO and IVMO, respectively),[31] spin-orbit splitting (ΔE_{sl}), multiplet splitting (ΔE_{ms}), charge inducing (ΔE_{ind}), many-body perturbation (ΔE_{sat}), dynamic effect (gigantic Coster-Kronig transitions), Auger process, etc.[32,33] If several of these effects show up in the XPS spectrum for a certain electronic level simultaneously at a comparable probability, the correct interpretation of the spectrum is not possible. If the probabilities are not equal, the correlation of the XPS structure parameters with physical and chemical properties of the studied compound can be drawn. In this case, the XPS structure parameters can characterize the following: degree of delocalization and participation of electrons in a chemical bond, electronic configuration and oxidation states of ions, uncoupled electron density at paramagnetic ions, degree of participation of the filled electronic shells of metals and ligands in the IVMO and the OVMO formation, the IVMO and the OVMO structures and nature, local environment structure, etc.[31–33]

The BE range of 0 eV to ∼35 eV is especially important since the XPS in this range reflects the MO structure and the valence electronic states densities (with the photoemission cross sections in mind); however, the interpretation of the XPS structure in this BE range requires an understanding of how effective a certain extra structure formation mechanism is. To evaluate the contributions of different structure formation mechanisms to the valence XPS structure, one has to study the core (35 eV–1250 eV) XPS structures.[31–33]

When doing the XPS study of oxygen-containing actinide compounds, it was found that in the ∼15 eV–∼35 eV BE range, peaks are several electron volts wide, which sometimes is wider than the corresponding core electron peaks.[31,33] For example, the O $1s$ ($E_b = 530.1$ eV) full width at half-maximum (FWHM) (Γ, eV) peak for PuO_2 is $\Gamma = 1.1$ eV, while the corresponding O $2s$ ($E_b \sim 22$ eV) peak is ∼4 eV wide and structured. It contradicts the Heisenberg uncertainty ratio

$\Delta E\,\Delta\tau \approx h/2\pi$, where ΔE is the natural width of a level from which an electron was extracted, $\Delta\tau$ is the hole lifetime, and h is the Planck constant. Since the hole lifetime ($\Delta\tau$) grows as the absolute atomic level energy decreases, the lower BE XPS atomic peaks are expected to be narrower. For PuO_2 (Ref. 19) and other actinide oxides (Ref. 33), it is vice versa. This fact stimulated experimental and theoretical studies of the low BE (∼15 eV–∼35 eV) XPS structure in oxides of actinides,[33] lanthanides,[32] and other compounds.[31] One of the reasons for such an XPS structure formation was the IVMO formation with significant participation of the An 6*p*- and O 2*s*-filled atomic shells.[31,33] Practically, the low energy spectra reflect the valence band (0 eV–∼35 eV) structure. They are observed as several electron volt–wide bands. The IVMO were shown to form in compounds of lanthanides[32] and other elements.[31]

The XPS of the low BE (0 eV–∼35 eV) electrons from PuO_2 (Refs. 20 and 22) were measured, and the theoretical calculations of the electronic structure of PuO_2 in this energy range in the nonrelativistic (NR) approximation of the X_α discrete variation method (X_α DVM)[34] and in the quasirelativistic cluster approximation of the quasirelativistic extended Huckel method,[22] as well as in the density functional theory (DFT) approximation,[35] were done previously. The calculations allowed only a qualitative interpretation of the low BE XPS from PuO_2. Unfortunately, the up-to-date relativistic calculation results for PuO_2 (Refs. 36–46) for the BE range of 0 eV–∼15 eV did not take into account the overlapping of the inner valence Pu 6*p* and the O 2*s* atomic orbitals (AOs) and, therefore, did not allow a correct valence (∼15 eV–∼35 eV) XPS structure interpretation.

At the present time, the quantitative interpretation of the valence XPS structure in the BE range of 0 eV–∼35 eV, which takes into account the photoelectron, conversion, emission, and other x-ray spectral data and relativistic calculation results, was done for ThO_2 (Ref. 47), UO_2 (Ref. 48), ThF_4 (Ref. 49), UF_4 (Ref. 50), UO_2F_2 (Ref. 51), and γ-UO_3 (Ref. 52). The present work analyzed the XPS from PuO_2 in the BE range of 0 eV–1250 eV and quantitatively interpreted the XPS structure in the BE range of 0 eV–∼35 eV, taking into account the photoelectron,[5–7] Auger, and other x-ray spectra[53] data. The BEs and core electron spectral structure parameters as well as the self-consisting field relativistic discrete variation (SCF RDV) calculation results for the PuO_8 (D_{4h}) cluster reflecting Pu close environment in PuO_2 were taken into consideration.

II. EXPERIMENTAL

A. Samples

PuO_2 samples for the XPS study were prepared by oxalate technique and by electrolysis as dense thin layers (Ø3–4 mm) on the Pt substrate (Ø14-mm foil).

1. Pu synthesis from oxalate

The standard nitrate ^{239}Pu solutions were used for sample preparation. The volumes of the solutions were calculated so that the yield was not less than 50% and that not less than $10^{18}-10^{19}$ Pu atoms were on the platinum substrate. Deionized water and chemically pure reagents were used.

Oxalic acid in double excess to Pu was added to a nitric ^{239}Pu(IV) solution and thoroughly mixed. The precipitate was separated by centrifugation and washed three times in ethanol. Several drops of water were added to the obtained $Pu(C_2O_4)_4$ precipitate, and the suspension gradually put on the substrate. Afterward, the sample on the substrate was left under a 500 W incandescent lamp to dry. Then the sample was annealed in a muffle furnace according to the following program: 20 hours heating to 700 °C; 5 hours heating from 700 °C to 1200 °C; 10 hours annealing at 1200 °C; and 15 hours cooling from 1200 °C to room temperature. Tetravalent plutonium-oxalate decomposition reaction is seen in Eq. (1):

$$Pu(C_2O_4)_4 \xrightarrow{t^\circ} PuO_2 + 6CO_2 \uparrow + 2CO \uparrow . \qquad (1)$$

2. Electrolytic synthesis of PuO_2

A nitric plutonium solution of $\sim 10^{18-19}$ atoms was placed in the electrolytic cell with platinum substrate as a cathode. Platinum wire was used as an anode; ammonium nitrate (NH_4NO_3) was used as an electrolyte. The process was carried out at 1 A and 30 mV for 1–2 hours until the plutonium was extracted completely from the solution. Aliquots of 20 μl were taken periodically to control the plutonium content in the solution by liquid scintillation spectrometry. After the electrolysis was completed, the sample on the substrate was placed in a muffle furnace and annealed by the same program used for oxalate decomposition.

PuO_2 formation on the substrate surface was controlled by scanning electron microscopy and XPS. To prepare the PuO_2 sample for the XPS study, the surface was etched with Ar ions at 2.5 KeV and 10 μA from 10 seconds to 2 minutes. The XPS studies of the sample surface were done after 1 day and 1 month in the air to develop the technique of preparation of samples close to their stoichiometric compositions to PuO_2. The XPS data for these two measurements did not differ within the 10% measurement error.

B. X-ray photoelectron measurements

XPS spectra of PuO_2 were measured with an electrostatic spectrometer (Quantera SXM) using $AlK_{\alpha 1,2}$ ($h\nu = 1486.6$ eV) radiation (Ø50 μm beam) under 1.3×10^{-7} Pa at room temperature. The device resolution measured as the FWHM of the Au $4f_{7/2}$ peak was 0.7 eV. The BE E_b(eV) was measured relative to the BE of the C 1*s* electrons from hydrocarbons absorbed on the sample surface that were accepted to be equal to 285.0 eV. The C 1*s* XPS peak from hydrocarbon on the sample surface was observed at low intensity and at 1.3 eV wide.[33] The error in the determination of the BE and the peak widths did not exceed ±0.1 eV, and the error of the relative peak intensity − ±10%. Shirley[54] subtracted the elastically scattered electrons-related background.

The valence and the core electron XPS structure for PuO_2 in the BE range of 0 eV–1250 eV is both typical and distinctive. It confirms unambiguously the presence of PuO_2 on the substrate surface (see Table I). The studied samples were proven not to contain more than 0.1 at.% of impurities since foreign peaks were not observed in the whole XPS BE range of 0 eV–1250 eV. However, a low intense Pt $4f$ doublet at E_b(Pt $4f_{7/2}$) = 70.8 eV and $\Delta E_{sl} = 3.3$ eV occasionally showed up.

TABLE I. Electron BE E_b (eV) and photoionization cross sections σ[a] at 1487 eV.

Pu *nlj* O *nlj*	PuO_2	PuO_2[b]	Pu[c]	Pu_{Theor}[d]	σ
Pu $5f$	2.6 (2.5)		~0.6	0.6	25.5
Pu $6p_{3/2}$	17.9 (2.8)	18.1	17.2	18.6	5.20
Pu $6p_{1/2}$	30.1(2.5)	30.3	29.2	30.5	1.76
			32.0		
Pu $6s$	50.1(4.0)		45.2		
			52.7	51.7	2.33
Pu $5d_{5/2}$	104.6	104.7	101.3	103.1	51.2
Pu $5d_{3/2}$			113.7	118.9	34.8
Pu $5p_{3/2}$	210.5	215.9	211.1	220.5	32.5
	215.5				
Pu $5p_{1/2}$	278.7 (2.9)		284.2	285.4	9.23
Pu $5s$			353.1	355.6	10.4
			365.1		
Pu $4f_{7/2}$	426.1(2.0)	426.3	422.1	422.4	424
Pu $4f_{5/2}$	438.8(1.9)	439.0	435.1	436.2	333
Pu $4d_{5/2}$	801.4(6.0)	801.5	798.1	802.2	243
Pu $4d_{3/2}$	849.4 (6.0)	849.5	844.8	850.3	158
Pu $4p_{3/2}$	1125.1(6.8)		1122.6	1127.7	109
O $2p$	~4.9				0.27
O $2s$	22.4	22.5			1.91
O $1s$	530.1(1.1)	530.0			40

[a]Photoionization cross sections σ (kiloBarn per atom) from Ref. 65.
[b]Values given relative to the C $1s$ BE E_b(C $1s$) = 285.0 eV from Ref. 20.
[c]Values for metallic Pu from Ref. 10.
[d]Calculation data from Ref. 64, values given relative to the Pu $5f$ peak from metallic Pu.

It evaluated the Pt $5d^9$ contribution to the PuO_2 valence band (0 eV–10 eV BE) XPS intensity as several percentage points and was taken into account. The core and valence XPS from metallic Pt were taken. BE E_b(Pt $4f_{7/2}$) = 70.8 eV, spin-orbit splitting ΔE_{sl}(Pt $4f_{7/2}$) = 3.3 eV, and the FWHM Γ(Pt $4f_{7/2}$) = 0.9. The valence band was observed in the BE range of 0 eV–10 eV with peaks at 0.2, 1.4, and 4.0 eV, general FWHM Γ(VB) = 5.8 eV, and the valence band to the Pt $4f_{7/2}$ peak intensity ratio I(VB)/I(Pt $4f_{7/2}$) = 0.16.

The quantitative elemental analysis of several nanometer-deep layers of the studied samples was done. It was based on the fact that the spectral intensity is proportional to the number of certain atoms in the studied sample. The following equation was used: $n_i/n_j = (S_i/S_j)(k_j/k_i)$, where n_i/n_j is the relative concentration of the studied atoms, S_i/S_j is the relative core-shell spectral intensity, and k_j/k_i is the relative experimental sensitivity coefficient. The following coefficients relative to the C $1s$ were used: 0.25 (C $1s$), 0.70 (O $1s$), and 10.21 (Pu $4f_{7/2}$; see, e.g., Refs. 55 and 56). The best stoichiometric composition of plutonium dioxide was $PuO_{2.02}$, taking into account the O $1s$ and Pu $4f_{7/2}$ peaks.

III. CALCULATIONS

The electronic structure calculations of PuO_2 were made for the three types of finite fragments of crystal lattice: a 279-atom cluster $Pu_{63}O_{216}$, a 69-atom cluster $Pu_{13}O_{56}$, and a PuO_8 cluster. The last object modeled the closest Pu environment to PuO_2. The PuO_2 crystal structure parameters corresponded to Ref. 57 ($R_{Pu\text{-}O}$ = 0.2337 nm). For the modeling of boundary conditions for the $Pu_{63}O_{216}$ and $Pu_{13}O_{56}$ fragments, we used an extended cluster scheme, described in detail in Ref. 58. In this model, the crystal fragment under study consists of two parts: the internal main part (or the core of the cluster) and the outer part (or the shell). The latter part usually includes the atoms of 1–5 coordination spheres surrounding the core. During the self-consistency procedure, the electron densities and the potential of the ions in the shell are replaced by the corresponding values obtained for the crystallographically equivalent centers of the cluster core. In addition to introducing the long-range component of the surrounding crystal potential, the extended cluster is embedded in a pseudopotential of the outer crystal lattice, including several thousand centers with Coulomb and exchange-correlation potentials obtained for the corresponding equivalent atoms in the internal part of the cluster. This pseudopotential modeling of the long-range crystal potential usually improves convergence and becomes very important in the calculations of compounds with noticeable charges on atoms, such as oxides and fluorides.

In the case of $Pu_{63}O_{216}$, the core of the cluster included the Pu atom in the center (Pu_1), with eight nearest oxygen neighbors (O_1) and 12 plutonium sites of the next metal coordination sphere with their 48 nearest oxygen atoms. The other atoms of the cluster formed the shell, and during self-consistency, their electronic densities and potentials were kept equivalent to those of Pu_1 and O_1. The smaller $Pu_{13}O_{56}$ fragment is actually the main part of $Pu_{63}O_{216}$, where 48 outer ligands now form the shell around the PuO_8Pu_{12} core; during self-consistency, their densities and potentials were kept equivalent to those of O_1. The rest sites of $Pu_{63}O_{216}$ cluster were added to the pseudopotential part of boundary condition. In the case of the simplest fragment PuO_8, the renormalization procedure for the oxygen atom's valence AO populations during self-consistency was used in the calculations. The latter model of small cluster boundary condition also allows one to include into the iterative scheme the stoichiometry of the compound and the possibility of charge redistribution between outer atoms in the cluster and the surrounding crystal.

In this paper, the electronic structure is calculated in the DFT approximation using the original code of the fully RDV cluster method[59,60] with exchange-correlation potential.[61] The RDV method is based on the solution of the Dirac-Slater equation for four-component wave functions transforming according to the irreducible representations of the double point group (D_{4h} in the present calculations). For the calculation of symmetry coefficients, we used the original code, which uses the projection operators technique[59] and includes the matrices of irreducible representations of double point groups[62] and the transformation matrices presented in Ref. 63. The extended basis of four-component numerical AOs obtained as the solution of Dirac-Slater equation for the isolated neutral atoms also included the Pu $7p_{1/2}$ and the Pu $7p_{3/2}$ functions in addition to the occupied AOs. The use of such "most natural basis orbitals" and the absence of any muffin-tin approximation to potential and electronic density allow one to describe the formation of interatomic bonds. In such an approach, this description is more illustrative than that

obtained in the band structure approach. Numerical diophantine integration in matrix elements calculations was carried out for 700 000 ($Pu_{63}O_{216}$), 178 000 ($Pu_{13}O_{56}$), and 22 000 (PuO_8) sample points distributed in the cluster space. It provided the convergence of MO energies better than 0.1 eV.

IV. RESULTS AND DISCUSSION

As mentioned above, the valence XPS structure of PuO_2 in the range of 0 eV–∼35 eV reflects the MO structure. The contributions of other mechanisms to this XPS structure formation have to be taken into account also. Therefore, it takes analysis of the core-level XPS structure.

A. Core electron XPS structure of PuO_2

The electron BEs in the range of 0 eV–1250 eV measured in the present paper (Table I), for metallic plutonium,[10] calculation results for atomic Pu (Ref. 64), and plutonium dioxide (Ref. 20), as well as the photoionization cross-sections,[65,66] are given in Table I.

The O 1*s* XPS of PuO_2 was observed as a single peak at E_b(O 1*s*) = 530.1 eV and FWHM Γ(O 1*s*) = 1.1 eV with a shoulder at E_b(O 1*s*) = 531.6 eV at the higher BE side from the basic peak (Fig. 1; Table I). This shoulder was attributed to hydroxyl groups, while the one at E_b(O 1*s*) = 532.5 eV was attributed to water on the sample surface. The peak intensity ratio yielded 87% of PuO_2, 10% of OH^-, and 3% of H_2O. These data agree with the results for PuO_2 on the Pt substrate[20] as well as for PuO_2 formed on the surface of metallic Pu (Ref. 22). The O 2*p* and the O 2*s* intensities from the impurities increase the error during the valence XPS decomposition.

The Pu 4*f* XPS from PuO_2 at the highest probability shows the many-body perturbation-related structure attributable to an extra electronic transition within the filled and vacant valence levels during the Pu 4*f* photoemission. It appears as shake-up satellites, whose parameters reflect the MO structure. As a result, the Pu 4*f* XPS consists of the spin-orbit split doublet with ΔE_{sl}(Pu 4*f*) = 12.7 eV, and the shake-up satellites at the higher BE side with ΔE_{sat} = 6.9 eV (Fig. 2; Table I). The satellite intensity ($I_{sat} = I_s/I_o$) calculated as the ratio of the XPS satellite area (I_s) to the basic peak area (I_o) was 18%. The Pu 4*f* structure is typical for the Pu(IV) oxidation state.[1,20,22,23,26,27,33] For the first half of the lanthanide compound row, the shake-up satellites appear in the core-level XPS, and their intensity drops as the BE of the level decreases.[32] The same satellites are expected in the other core-level XPS from PuO_2. Indeed, the Pu $4d_{5/2}$ XPS [E_b(Pu $4d_{5/2}$) = 801.4 eV and Γ(Pu $4d_{5/2}$) = 6.0 eV] exhibits shake-up satellites at ΔE_{sat}(Pu $4d_{5/2}$) = 6.9 eV at the higher BE side from the basic peak. Its intensity was I_{sat} = 33% (Fig. 3). The similar satellite in the Pu $4p_{3/2}$ XPS [E_b(Pu $4p_{3/2}$) = 1125.1 eV, Γ(Pu $4p_{3/2}$) = 6.8 eV; see Table I] was observed at ΔE_{sat}(Pu $4p_{3/2}$) = 6.9 eV, and its intensity was I_{sat} = 47% (Fig. 4). The extrapolation of the shake-up satellite intensity ($I_{sat} = 0.04E_b + 0.18$) predicts the shake-up satellite intensity in the valence band XPS not to exceed several percentage points (Fig. 5). In reality, the shake-up satellite relative intensities in the valence spectral BE range

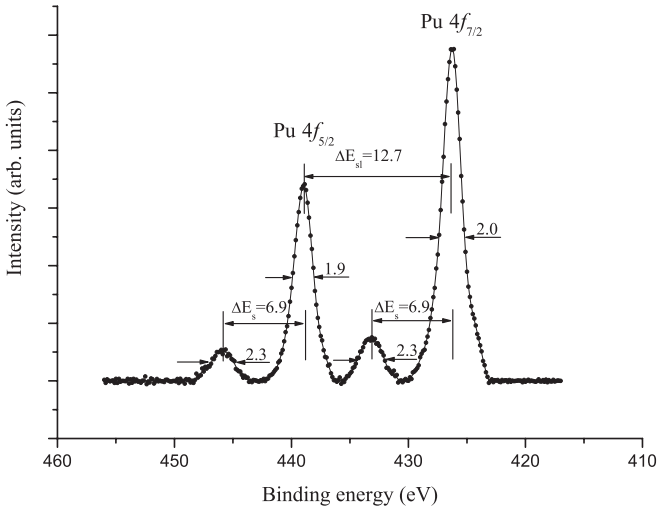

FIG. 2. Pu 4*f* XPS from PuO_2.

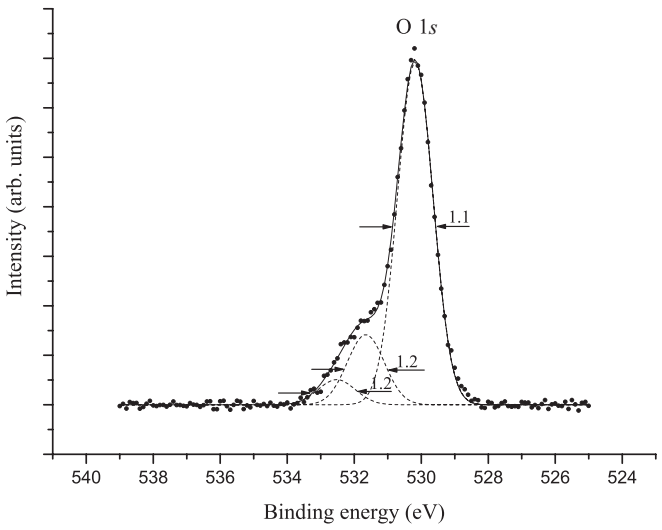

FIG. 1. O 1*s* XPS from PuO_2.

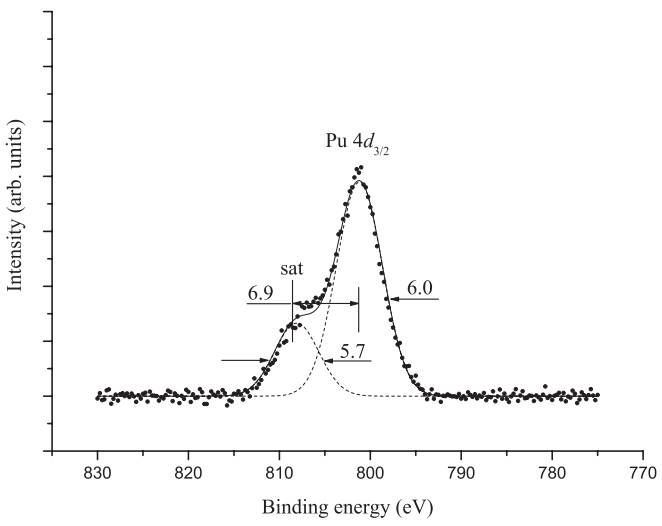

FIG. 3. Pu $4d_{5/2}$ XPS from PuO_2.

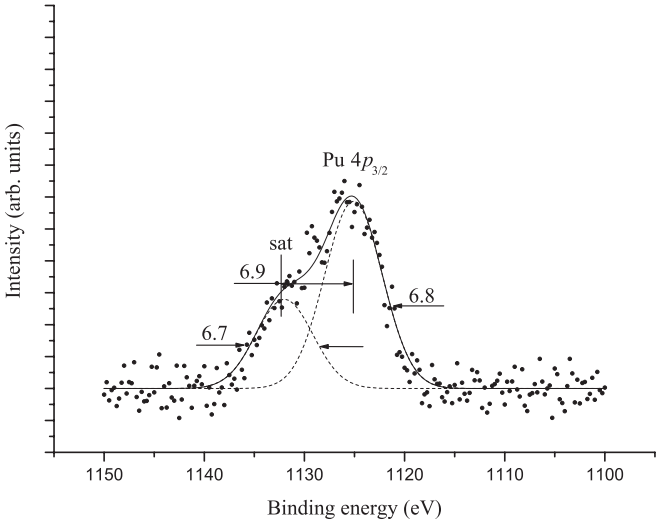

FIG. 4. Pu $4p_{3/2}$ XPS from PuO_2.

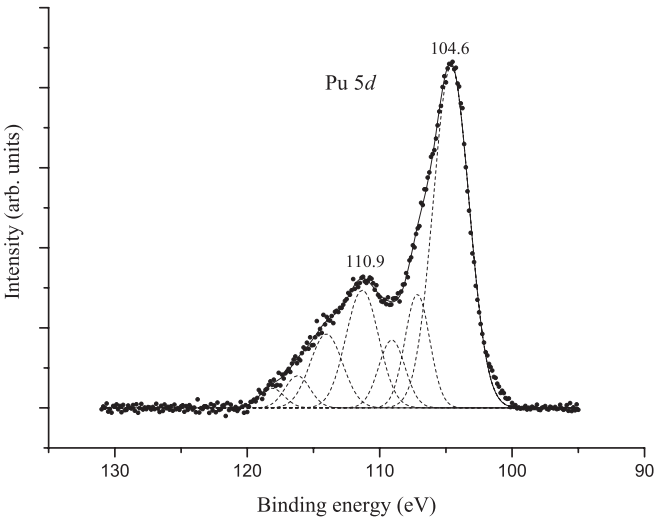

FIG. 6. Pu $5d_{5/2}$ XPS from PuO_2.

can be higher since the measurement error can exceed 10% (see Fig. 5).

The multiplet splitting caused by the presence of the uncoupled Ln $4f$ electrons in lanthanide compounds results in the Ln $4d$ XPS structure.[32] Therefore, the multiplet splitting was expected to show up with the higher probability in the Pu $5d$ XPS (Refs. 20 and 33). Indeed, the Pu $5d$ spectrum instead of a spin-orbit split doublet [ΔE_{sl}(Pu $5d$)$_{theor}$ = 15.8 eV (Ref. 64)] exhibits a complicated structure with the Pu $5d_{5/2}$ maximum at 104.6 eV (Fig. 6). This structure can be explained by the multiplet splitting superimposed with the shake-up satellites. Therefore, it is difficult to separate the satellite-related structure and to determine the satellite intensities. The multiplet splitting is very likely to show up in the Ln $4s$ XPS from lanthanide oxides.[32] In the Ln $5s$ XPS, it is more than twice lower than in the Ln $4s$ XPS. Therefore, the Pu $5s$ and Pu $6s$ XPS are expected to exhibit the multiplet splitting.

The dynamic effect is related to the gigantic Coster-Kronig transitions, e.g., the one observed in the Pu $5p$ XPS (Fig. 7). It shows up as the two peaks in the Pu $5p_{3/2}$ component at 210.5 eV and 215.7 eV. With the data on the Ln $4p$ XPS in mind,[32] one can attribute the Pu $5p$ XPS structure to the dynamic effect resulting in the complex Pu ion final state (ground final state: Pu $5p^5 5d^{10} 5f^n$; excited two-hole final state: Pu $5p^6 5d^8 5f^{n+1}$). This suggestion is based on the correlation of the Pu $5p$ and Pu $5d$ BEs: E_b(Pu $5p_{3/2}$) $\sim$ 213 eV and E_b(Pu $5d_{5/2}$) = 104.6 eV, which is close to the condition E_b(Pu $5p_{3/2}$) $\approx 2 \times E_b$(Pu $5d_{5/2}$). As a result, the probability of the extra two-hole final state Pu $5p^6 5d^8 5f^{n+1}$ grows.

The Pu $5s$ XPS is expected to be E_b(Pu $5s$) $\sim$ 359 eV. For metallic Pu, it was observed in the range of $\sim$35 eV and contained two structured peaks at 353.1 and 365.1 eV ($\Gamma \sim$ 10 eV)[10] (Table I). This structure can be attributed to both the multiplet splitting and the dynamic effect.[33] In this paper, it did not allow a reliable measurement of the Pu $5s$ XPS. The Pu $6s$ XPS exhibits a widened [Γ(Pu $6s$) = 4.0 eV] structured line at 50.1 eV, which is attributed to the dynamic effect resulting in the interaction of the configurations of the Pu final states, such as Pu $6s^1 6p^6 5f^n$ and Pu $6s^2 6p^4 5f^{n+1}$. Indeed, for the

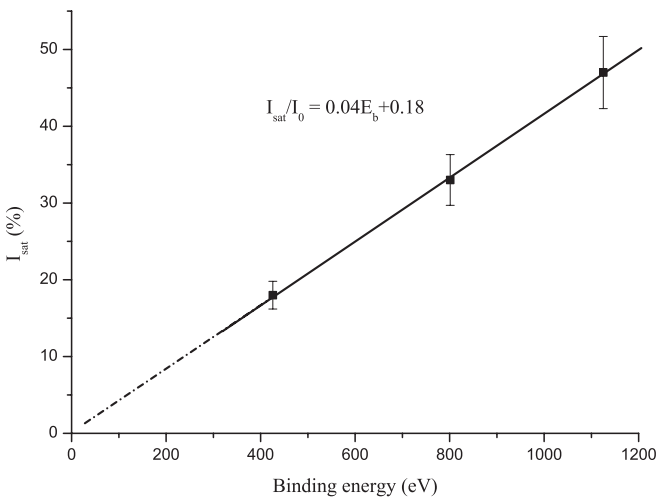

FIG. 5. Dependence of the shake-up satellite intensities (I_{sat} = I_s/I_0) on electron BE E_b(eV) in PuO_2.

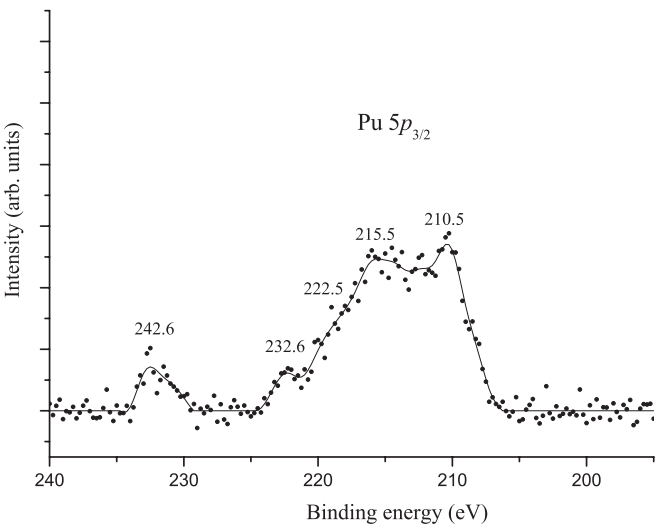

FIG. 7. Pu $5p_{3/2}$ XPS from PuO_2.

BEs of E_b(Pu 6s) = 50.1 eV, E_b(Pu 6$p_{3/2}$) = 17.9 eV, and E_b(Pu 6$p_{1/2}$) = 30.1, the condition E_b(Pu 6s) $\approx 2 \times E_b$(Pu 6p) is met. This spectrum can also exhibit the multiplet splitting and the shake-up satellite–related structures. Therefore, the Pu 6s XPS parameters cannot yield the conclusion on the possible participation of the Pu 6s electrons in the MO formation. The measured BEs and the observed Pu 4f, 5$p_{3/2}$, 5d XPS structures agree with the previously obtained results for PuO_2 (Ref. 20).

Since the An 6p XPS structure ongoing from ThO_2 to PuO_2 does not change significantly while the number of the quasiatomic An 5f electrons grows from 0 to 4 (Refs. 20 and 33), one can suggest that the multiplet splitting does not play a primary role in the valence XPS structure formation in the BE range of ~15 eV–~35 eV. The dynamic effect-related structure is also a low probability in this BE range because of the atomic states, but the quasiatomic Pu 5f ones are absent in the valence band. As a result, a suggestion that the valence XPS structure in a high degree can be attributed to the MO formation, except for the peak at 9.8 eV, can be drawn. The peak at 9.8 eV is ~7 eV away from the peak of the localized Pu 5f electrons [E_b(Pu 5f) = 2.6 eV, see Table I] and, therefore, can be admittedly attributed to the many-body perturbation (shake-up satellite).

For the interpretation of the MO-related valence band XPS structure, the results of electronic structure calculations of the finite clusters in PuO_2 were used.

B. Electronic structure of the clusters in PuO_2

Plutonium atom ground-state configuration $^7F_0$ can be presented as [Rn]$6s^2 6p^6 5f^6 6d^0 7s^2 7p^0$, where [Rn] is the radon electronic configuration and the other electronic shells are valence and can participate in the MO formation.[31,33] The total densities of states (DOS) obtained for the central Pu_1 and O_1 atoms in the three clusters are shown in Fig. 8. A comparison of the DOS in Fig. 8 shows that the set of discrete molecular levels in small PuO_8 fragments (we have broadened each MO level with a Lorentzian function of constant width

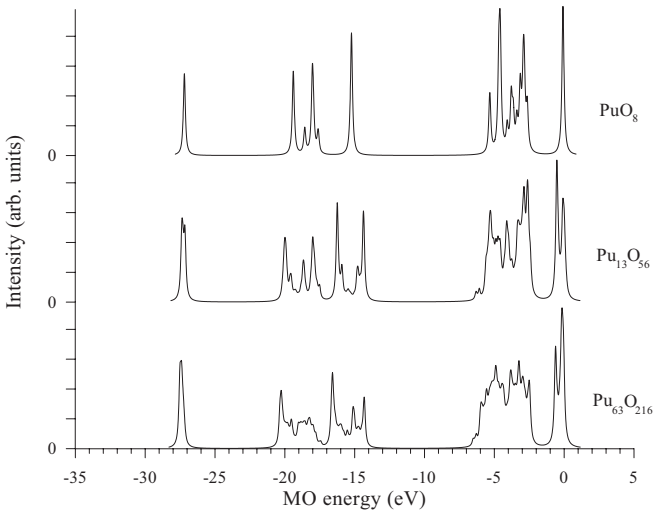

FIG. 8. Total DOS for the central part of PuO_8, $Pu_{13}O_{56}$, and $Pu_{63}O_{216}$ clusters obtained in RDV calculations.

for all MOs) transforms to rather real energy bands of various widths in the large $Pu_{63}O_{219}$ cluster. Surprisingly, the positions of gravity centers of the main bands in all fragments are close to each other. Moreover, the analysis of the covalent mixing of the Pu 6$p_{1/2}$, 6$p_{3/2}$ with the O 2s orbitals and the Pu 5$f_{5/2}$, 5$f_{7/2}$, 6$d_{3/2}$, 6$d_{5/2}$, 7s, 7$p_{1/2}$, 7$p_{3/2}$ with the O 2p AOs shows that the primary features of hybridization between metal and oxygen states are also similar in three clusters. Since the 279- and 69-atomic fragments in the energy region under investigation (0–35 eV) contain 2357 and 577 orbitals, respectively, for the illustration of general structure of the primary molecular states, we use the results of the RDV calculations for the smallest PuO_8 cluster, which models only the closest environment of Pu in PuO_2. The characteristics of all vacant and occupied MOs in the energy region from 0–50 eV obtained for this cluster are given in Table II.

The RDV method is based on the MO as linear combinations of AOs (LCAO) approach, which allows one to use both atomic and molecular terms for the chemical bond description. Indeed, the OVMOs and the IVMOs are formed during the chemical bond formation and the overlap of AOs of the neighboring plutonium and oxygen atoms. These MOs, in addition to the Pu 6s, 6p, 5f, 6d, and 7s, and the O 2s, 2p AOs also contain the Pu 7p states, which are vacant in the isolated plutonium atom. In contrast to the results of the NR calculations of PuO_2 (Ref. 34), which show a significant participation of the Pu 6s AOs in the MO formation, the results of relativistic calculations show that the Pu 6s AOs participate insignificantly in the MO formation (Table II). However, the Pu 7s and the Pu 7p AOs participate significantly in the MO formation. While the contributions from the Pu 5f AOs were obtained mostly in the OVMO bands, the Pu 6p and 6d AOs participate in both the OVMO and the IVMO states. Especially significant mixing of the Pu 6$p_{3/2}$ and the O 2s AOs was observed for the $17\gamma_6^-$, $13\gamma_7^-$ (5) and $15\gamma_6^-$, $11\gamma_7^-$ (8) IVMOs (Table II; Figs. 9 and 10). The mixing of the Pu 6$p_{1/2}$ and the O 2s AOs for the $16\gamma_6^-$ (6) and $14\gamma_6^-$ (9) IVMOs takes place in lesser extent than in the corresponding orbitals in ThO_2 (Ref. 47) and UO_2 (Ref. 48). This result can be explained by the increase of the spin-orbit splitting ΔE_{sl}(An 6p) and by the increase of the An 6$p_{1/2}$ BE with respect to that of the O 2s AOs as the atomic number Z grows in the actinide row. These results allow an interpretation of the valence XPS structure of PuO_2.

C. Valence XPS structure of PuO_2

The XPS from PuO_2 in the BE range of 0 eV–~35 eV can be conditionally subdivided into two ranges (Fig. 9). The first range of 0 eV–~15 eV exhibits the OVMO-related structure. These OVMOs are formed mostly from the Pu 5f, 6d, 7s, 7p, and the O 2p AOs of the neighboring atoms. The second range of ~15 eV–~35 eV exhibits the IVMO-related structure. These IVMOs appear in a higher degree due to the strong interaction of the completely filled Pu 6p and O 2s AOs. The OVMO XPS structure has its typical features and can be subdivided into the four explicit components (1–4; Fig. 9). The results of the PuO_2 outer valence XPS decomposition into three peaks at 2.6, 4.9, and 6.6 eV (Fig. 9; Table III) agree with the photoelectron spectral data for plutonium dioxide.[1,5–7] These

TABLE II. MO composition (parts) and energies E_0[a], eV for the PuO_8 cluster (RDV), and photoionization cross sections σ_i[b].

			MO Composition												
			Pu										O		
	MO	$-E_0$, eV	$6s$ σ_i 1.15	$6p_{1/2}$ 0.87	$6p_{3/2}$ 1.29	$6d_{3/2}$ 0.63	$6d_{5/2}$ 0.57	$7s$ 0.11	$5f_{5/2}$ 4.26	$5f_{7/2}$ 3.96	$7p_{1/2}$ 0.05	$7p_{3/2}$ 0.06	$2s$ 0.96	$2p_{1/2}$ 0.07	$2p_{3/2}$ 0.07
OVMO	22 γ_7^+	−8.99					0.85						0.05	0.08	0.02
	25 γ_6^+	−8.77				0.45	0.39						0.05	0.01	0.10
	21 γ_7^+	−8.76				0.45	0.39						0.05	0.02	0.09
	24 γ_6^+	−6.43						0.89					0.06	0.02	0.03
	28 γ_6^-	−5.51								0.01	0.91		0.04	0.02	0.02
	20 γ_7^+	−5.42				0.39	0.46							0.04	0.11
	23 γ_6^+	−5.41				0.39	0.46							0.04	0.11
	27 γ_6^-	−4.11										0.92	0.03		0.05
	24 γ_7^-	−4.25										0.92	0.03		0.05
	23 γ_7^-	−1.79							0.07	0.74			0.01	0.10	0.08
	26 γ_6^-	−1.11								0.90				0.06	0.04
	22 γ_7^-	−1.11							0.01	0.90				0.02	0.07
	25 γ_6^-	−1.10								0.90				0.04	0.06
	21 γ_7^-	−0.15							0.72	0.12				0.02	0.14
	24 γ_6^-[c]	0.00							0.85	0.01				0.01	0.13
	20 γ_7^-	0.01							0.85	0.01				0.01	0.13
	23 γ_6^-	2.56												0.31	0.69
	19 γ_7^-	2.57												0.31	0.69
	22 γ_6^+	2.78												0.16	0.84
	19 γ_7^+	2.78												0.14	0.86
	21 γ_6^+	2.80												0.65	0.35
	22 γ_6^-	2.85			0.04				0.09	0.03				0.18	0.66
	18 γ_7^-	2.85			0.04				0.09	0.03				0.32	0.52
	18 γ_7^+	3.04												0.04	0.96
	17 γ_7^+	3.07												0.50	0.50
	20 γ_6^+	3.08												0.50	0.50
	21 γ_6^-	3.31		0.01						0.09	0.01			0.78	0.11
	17 γ_7^-	3.57							0.11	0.10				0.29	0.50
	16 γ_7^-	3.70			0.01				0.03	0.01		0.05		0.18	0.72
	20 γ_6^-	3.71			0.01				0.03	0.01		0.05		0.09	0.81
	19 γ_6^-	4.00		0.01							0.04		0.01	0.32	0.62
	16 γ_7^+	4.48				0.01	0.09						0.01	0.55	0.34
	19 γ_6^+	4.50				0.06	0.04						0.01	0.01	0.88
	18 γ_6^+	4.51				0.01		0.04					0.01	0.33	0.61
	15 γ_7^+	4.51				0.06	0.04						0.01	0.34	0.55
	15 γ_7^-	4.58							0.04	0.05				0.17	0.74
	18 γ_6^-	4.59							0.04	0.05				0.16	0.75
	14 γ_7^-	4.61							0.06	0.03				0.58	0.33
	14 γ_7^+	5.24				0.06	0.08							0.28	0.58
	17 γ_6^+	5.25				0.06	0.08							0.28	0.58
IVMO	17 γ_6^-	15.15			0.62							0.02	0.31	0.02	0.03
	13 γ_7^-	15.16			0.62							0.02	0.31	0.02	0.03
	12 γ_7^-	17.54							0.01	0.01			0.98		
	16 γ_6^-	17.89		0.02							0.04		0.94		
	13 γ_7^+	17.95					0.06						0.94		
	12 γ_7^+	17.96				0.03	0.03						0.94		
	16 γ_6^+	17.96				0.03	0.03						0.94		
	15 γ_6^+	18.50	0.01					0.07					0.92		
	15 γ_6^-	19.32			0.33							0.01	0.65		0.01
	11 γ_7^-	19.32			0.33							0.01	0.65		0.01
	14 γ_6^-	27.12		0.96									0.03		0.01
	14 γ_6^+	46.39	0.99										0.01		

[a]Levels shifted by 13.45 eV toward the positive values (upward).

[b]Photoionization cross sections σ_i (kiloBarn per electron) for O from Ref. 65 and Pu from Ref. 66.

[c]HOMO (highest occupied MO) (two electrons), occupation number for all the orbitals is 2.

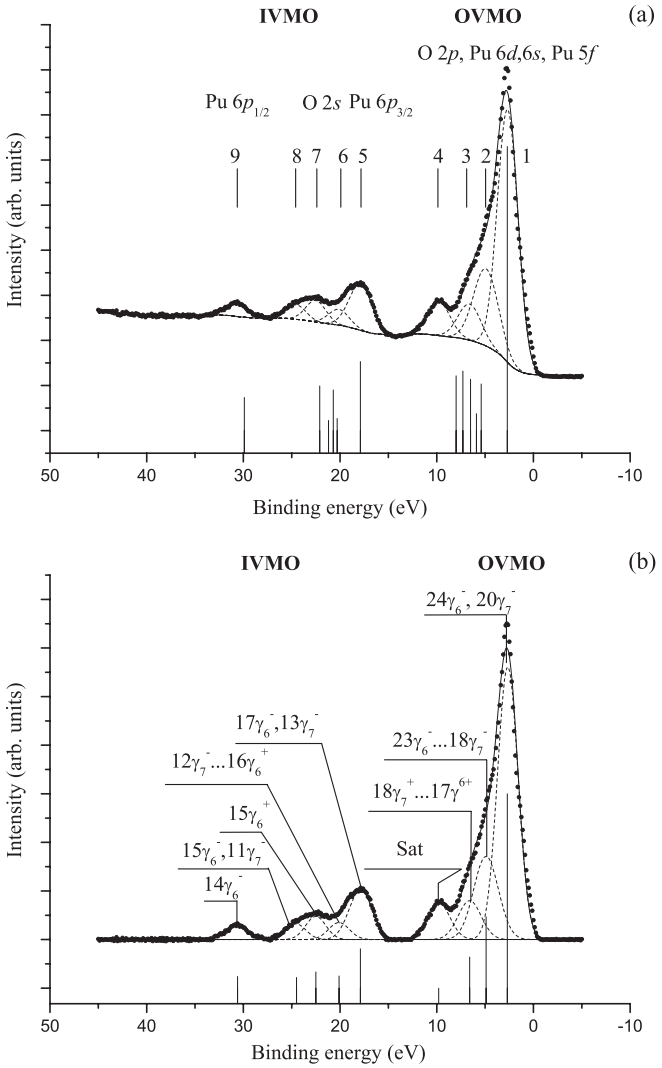

FIG. 9. Valence band XPS from PuO_2. (a) The spectrum with the secondarily scattered electron background. The dashed lines show the division of the spectrum into separate components; vertical bars show the calculated (RDV) spectrum. (b) The spectrum with subtracted background. The dashed lines show the division of the spectrum into separate components; vertical bars show the correct expected spectrum.

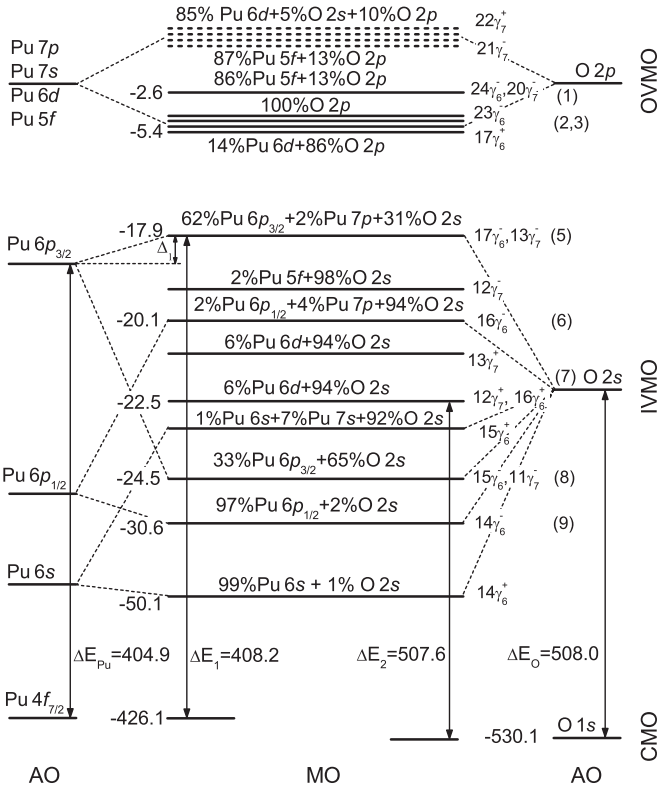

FIG. 10. MO scheme for the PuO_8 cluster obtained with the use of theoretical and experimental data. Chemical shifts are not indicated. Arrows show some measurable level BE differences. Experimental BEs (eV) are given to the left. The energy scale is not kept.

data also show three peaks at 2.5, 4.6, and ~6.5 eV (Ref. 6), but the XPS and photoelectron-peak intensities differ significantly. The reason is that the O $2p$ and the An $5f$ photoionization cross sections are comparable at the He II (40.8 eV) excitation, while at the AlKα (1486.6 eV), the An $5f$ photoionization cross section is about 50 times higher than the O $2p$ one (Table II).[66] The significant growth of the peak intensity at 2.6 eV as the excitation energy increases confirms experimentally that this peak originates primarily from the Pu $5f$ electrons.[4] This agrees with the calculation data (Tables II and III).

The IVMO range exhibits explicit peaks and can be subdivided into five components (5–9; Fig. 9). Despite the formalism of such a division, it allows a qualitative and quantitative comparison of the XPS parameters with the relativistic calculation results for the PuO_8 cluster.

Since photoemission results are given for an excited state of an atom with a hole on a certain shell, the calculations must be done for transition states for a stricter comparison of the theoretical and experimental BEs (Ref. 67). However, the valence electron BEs calculated for transition states are known to differ from the corresponding values for the ground state by a constant shift. Therefore, the present paper gives the calculated BEs (Table II) shifted by 2.75 eV (Table III). Taking into account the MO compositions (Table II) and the photoionization cross sections,[65,66] the theoretical intensities of several XPS ranges were determined (Table III). Comparing the experimental XPS and the theoretical data, one should keep in mind that the XPS from plutonium dioxide reflects the band structure and consists of bands widened due to the solid state effects. Despite this approximation, a satisfactory qualitative agreement between the theoretical and the experimental data was obtained [Fig. 9(a)]. Indeed, the corresponding theoretical and experimental FWHMs and relative intensities of the inner and the outer valence bands are comparable [Table III; Fig. 9(a)]. A satisfactory agreement between the experimental and calculated BEs of some MOs was also reached (Table III). The worst discrepancy was observed for the middle IVMO XPS ($12\gamma_7^- – 15\gamma_6^+$). As mentioned above, the NR X_α DVM (Ref. 34) and the REX (Ref. 22) results allowed only qualitative interpretation of the low BE XPS structure of PuO_2. The present relativistic calculations practically allow a quantitative identification of the valence XPS of PuO_2 in the whole BE range of 0 eV–~35 eV [Table III; Fig. 9(b)]. The expected

TABLE III. Valence XPS parameters for PuO_2 and for the PuO_8 cluster (RDV) and the Pu $6p$ and Pu $5f$ electronic state density ρ_i (e^-).

			XPS						
			Energy[b], eV	Intensity,%		Pu $6p$,$5f$ electronic state density $\rho_i(e^-)$, e^- (electrons)			
	MO	$-E$[a], eV	Experiment	Theory	Experiment	$5f_{5/2}$	$5f_{7/2}$	$6p_{1/2}$	$6p_{3/2}$
OVMO	24 $\gamma_6{}^-$[c]	2.75	2.6 (2.5)	21.0	42.2	1.70	0.02		
	20 $\gamma_7{}^-$	2.76		21.0		1.70	0.02		
	23 $\gamma_6{}^-$	5.31		0.1					
	19 $\gamma_7{}^-$	5.32		0.1					
	22 $\gamma_6{}^+$	5.53		0.1					
	19 $\gamma_7{}^+$	5.53		0.1					
	21 $\gamma_6{}^+$	5.55	4.9 (3.0)	0.1	15.5				
	22 $\gamma_6{}^-$	5.60		3.2		0.18	0.06		0.08
	18 $\gamma_7{}^-$	5.60		3.2		0.18	0.06		0.08
	18 $\gamma_7{}^+$	5.79		0.1					
	17 $\gamma_7{}^+$	5.82		0.1					
	20 $\gamma_6{}^+$	5.83		0.1					
	21 $\gamma_6{}^-$	6.06		2.2			0.18	0.02	
	17 $\gamma_7{}^-$	6.32		5.0		0.22	0.20		
	16 $\gamma_7{}^-$	6.45	6.6 (2.8)	1.1	6.8	0.06	0.02		0.02
	20 $\gamma_6{}^-$	6.46		1.1		0.06	0.02		0.02
	19 $\gamma_6{}^-$	6.75		0.4				0.02	
	16 $\gamma_7{}^+$	7.23		0.9					
	19 $\gamma_6{}^+$	7.25		0.4					
	18 $\gamma_6{}^+$	7.26		0.2					
	15 $\gamma_7{}^+$	7.26		0.4					
	15 $\gamma_7{}^-$	7.33		2.2		0.08	0.10		
	18 $\gamma_6{}^-$	7.34		2.2		0.08	0.10		
	14 $\gamma_7{}^-$	7.36		2.5		0.12	0.06		
	14 $\gamma_7{}^+$	7.99		0.6					
	17 $\gamma_6{}^+$	8.00		0.6					
	Sat		9.8 (2.7)		6.1				
	ΣI_i[d]			69.0	70.6	4.38	0.84	0.04	0.20
IVMO	17 $\gamma_6{}^-$	17.90	17.9 (2.8)	5.1	13.0				1.24
	13 $\gamma_7{}^-$	17.91		5.1					1.24
	12 $\gamma_7{}^-$	20.29		1.8		0.02	0.02		
	16 $\gamma_6{}^-$	20.64	20.1 (2.5)	1.5	4.0			0.04	
	13 $\gamma_7{}^+$	20.70		1.5					
	12 $\gamma_7{}^+$	20.71		1.5					
	16 $\gamma_6{}^+$	20.71	22.5 (2.4)	1.5	5.3				
	15 $\gamma_6{}^+$	21.25		1.5					
	15 $\gamma_6{}^-$	22.07	24.5 (2.4)	3.3	3.5				0.66
	11 $\gamma_7{}^-$	22.07		3.3					0.66
	14 $\gamma_6{}^-$	29.87	30.6 (2.5)	4.9	3.8			1.92	
	ΣI_i[d]			31.0	29.6	0.02	0.02	1.96	3.80
	14 $\gamma_6{}^+$	49.14	50.1 (4.0)	~6.1	~3.3				

[a]Calculated energies (Table II) shifted by 2.75 eV toward the negative values (downward) so that the 17 $\gamma_6{}^-$ MO energy is 17.9 eV.
[b]FWHM in eV given in parentheses.
[c]HOMO (highest occupied MO) (two electrons), occupation number for all the orbitals is 2.
[d]The sum of peak intensities and Pu $6p$, $5f$ electronic state densities.

correct spectrum obtained on the basis of the calculations and the experimental data is given in Table III and drawn under the XPS as vertical bars [Fig. 9(b)]. These data promote the RDV method and underlie the quantitative MO scheme for understanding the nature of interatomic bonding in PuO_2.

Thus, the outer valence band intensity is formed mostly from the outer valence Pu $5f$, $6d$, $7s$, $7p$, and O $2p$ AOs, and to a lesser extent from the inner valence Pu $6p$ and O $2s$ AOs. The Pu $5f$ electrons contribute significantly to the OVMO intensity (Tables II and III). Because the Pu $5f$ photoemission cross section is high (Table II), the Pu $5f$ electrons contribute significantly to the OVMO intensity if they do not lose the f nature. For example, the Pu $5f$ electrons can be promoted to the Pu $6d$ level first, and then they participate in the

chemical bond formation. They also can participate directly in the formation of the interatomic bond without losing the f nature. The electronic structure calculations for PuO_2 yielded that the Pu $5f$ electrons participate directly in the chemical bond formation (Table II). In the ionic approximation for plutonium electronic configuration Pu $6p^6 5f^6 6d^0 7s^2$ in PuO_2, the calculated OVMO/IVMO intensity ratio was found to be 2.39 (Ref. 68), which agrees with the corresponding theoretical value 2.23 and the experimental value 2.39 (Table III) to within the measurement error of ±10%. This intensity ratio is an important characteristic of the PuO_2 electronic structure. These results yield a conclusion that the Pu $5f$ electrons participate directly in the chemical bond formation in PuO_2 partially losing the f nature. These electronic states are located closer to the middle and the top of the outer valence band (Tables II and III); the Pu $6d$ electronic states are located at the bottom of the outer valence band. This agrees with the theoretical and the experimental data for ThO_2 (Ref. 69) and UO_2 (Ref. 48).

The peak at 9.8 eV in the OVMO XPS BE range of PuO_2 (Fig. 9), according to Ref. 20, was attributed to the multiplet splitting of the Pu $5f^4$ Pu(IV) spectrum. In this case, the similar peak should be observed also in the Pu $5f^5$ Pu(III) spectrum (see the data on the multiplet splitting for the $f^5 \rightarrow f^4$ transition).[20] However, the OVMO XPS BE range of Pu_2O_3 does not exhibit this peak.[22] Furthermore, since the Pu $4f$ XPS of Pu_2O_3 exhibits shake-up satellites at the lower energy of $\Delta E_{sat} = 4.4$ eV, the OVMO XPS BE range of Pu_2O_3 does not exhibit a peak at 9.8 eV (Ref. 22). This peak cannot be attributed to the O $2p$ states as it was noted in Ref. 29 because its intensity regarding the O $2s$ intensity is too high [see σ(O $2s$) and σ(O $2p$) in Tables I and II].

Taking into account the quasiatomic nature of the Pu $5f^4$ electrons in PuO_2, one can expect shake-up satellites at $\Delta E_{sat} \approx 6.9$ eV similar to those in the Pu $4f$ XPS (Fig. 2). Indeed, the considered peak was observed on the higher BE side from the Pu $5f$ peak 7.1 eV away at E_b(Pu $5f$) = 2.6 eV, which agrees with ΔE_{sat}(Pu $4f$) = 6.9 eV. The intensity of this satellite regarding the Pu $5f$ peak (peak 1 on Fig. 9) intensity is I_{sat} = 14% (see Table III). This value agrees qualitatively with the dependence in Fig. 5. It has to be noted that this dependence is approximate.

In the IVMO XPS BE range, a satisfactory agreement was reached, e.g., for the $17\gamma_6^-$, $13\gamma_7^-$ (5), and $14\gamma_6^-$ (9) MOs responsible for the width ΔE of this XPS IVMO band. The calculated ΔE_{theor} = 11.97 eV agrees with the experimental ΔE_{exp} = 12.7 eV (Table III). It has to be noted that the theoretical (2.23) and experimental (2.39) OVMO/IVMO intensity ratios are comparable; that is, it confirms relative correctness of the approximations used in the calculations. The calculated and the experimental relative intensities of individual IVMO peaks are in qualitative agreement only (Table III).

Taking into account the experimental BE differences between the outer and the core MOs in PuO_2 and metallic Pu (Ref. 10), as well as the relativistic calculation data for the PuO_8 cluster in the MO LCAO approximation, a quantitative MO scheme for PuO_2 was built (Fig. 10). This scheme enables one to understand the real XPS structure and the chemical bond nature in PuO_2. In this approximation, one can pick out the antibonding $17\gamma_6^-$, $13\gamma_7^-$ (5), and $16\gamma_6^-$(6) and the corresponding bonding $15\gamma_6^-$, $11\gamma_7$ (8), and $14\gamma_6^-$(9) IVMOs, as well as the quasiatomic $12\gamma_7^-$, $13\gamma_7^+$, $12\gamma_7^+$, $16\gamma_6^+$, and $15\gamma_6^+$ (7) MOs attributed mostly to the O $2s$ electrons. The experimental data show that the O $2s$-related quasiatomic IVMO BEs have to be close by magnitude. Indeed, the O $1s$ XPS of PuO_2 allows a suggestion that their chemical nonequivalence should not exceed ~1 eV, since the O $1s$ peak was observed to be symmetric and Γ = 1.1 eV wide. The O $2s$ BE has to be about 22.1 eV since the ΔE_O = 508 eV and the O $1s$ BE in PuO_2 is E_b = 530.1 eV (Figs. 2 and 10). The theoretical results agree partially with these data. Taking into account that the experimental ΔE_{Pu} = 404.9 eV (Ref. 10) is comparable to the corresponding calculated value of 403.8 eV (Ref. 64) and ΔE_1 = 408.2 eV, one can find that Δ_1 = 3.3 eV (Fig. 10). Since the BE difference between the $17\gamma_6^-$, $13\gamma_7^-$ (5), and $14\gamma_6^-$ (9) IVMO is 12.7 eV, the calculated Pu $6p$ spin-orbit splitting for atomic Pu (Ref. 64) is ΔE_{sl}(Pu $6p$) = 11.9 eV and the experimental one for metallic Pu is 12.0 eV (Ref. 10), the perturbation can be evaluated as Δ_1 = 0.7 eV, which does not agree with the corresponding value of 3.3 eV found from the BE difference between the core and valence MOs. This discrepancy, apparently, can be explained by the IVMO formation, and such a comparison cannot be quite correct. The IVMO FWHMs cannot yield a conclusion on the IVMO nature (bonding or antibonding); however, one can suggest that the admixture of 5% of the O $2p$ and 2% of the Pu $7p$ AOs in the $17\gamma_6^-$, $13\gamma_7^-$ (5) IVMOs lead these orbitals to the losing of their antibonding nature (Table II; Fig. 10; see also Ref. 31). Therefore, the quantitative MO scheme for PuO_2, which was built on the basis of the experimental and the theoretical data, allows one to understand the nature of chemical bond formation in PuO_2 and to interpret the structures of other x-ray spectra of PuO_2 as shown, for example, by the spectra peaks of the absorption, valence electron-resonant emission, resonant and nonresonant emission spectra, conversion spectra, and others for ThO_2 (Ref. 69), UO_2 (Ref. 48), and UF_4 (Ref. 50).

D. The O $2s$, $2p$ electronic state densities in PuO_2

Since the XPS reflects the general electronic state densities, taking into account the photoionization cross sections, it is a good idea to compare the XPS and the theoretical calculation results with other x-ray spectra using the MO scheme (Fig. 10). Thus, the O Kα x-ray emission spectrum (O Kα XES) characterizes the partially filled O $2p$ electronic state density, taking into account the emission cross sections.[53] The near O $1s$ edge x-ray absorption spectrum (XAS) with account of the absorption cross sections characterizes the partial vacant O $2p$ electronic state density in PuO_2 (Ref. 53). Together with the OVMO XPS (Fig. 9) and the theoretical calculation results on the O $2p$ electronic state density (Table II), these two spectra are shown in Fig. 11. The spectra were reduced to the unified scale, where E_b(O $1s$) = 530.1 eV, E_b(Pu $4f_{7/2}$) = 426.1 eV, and E_b(Pu $5f$) = 2.6 eV (Table I). These spectra intensities were not normalized. The calculated intensities (vertical bars) are given with the background equal to one scale division below zero (Fig. 11). It was done due to the low intensity of the vacant states (see Table II). It has to be noted that the comparison of the spectra from Fig. 11 and the

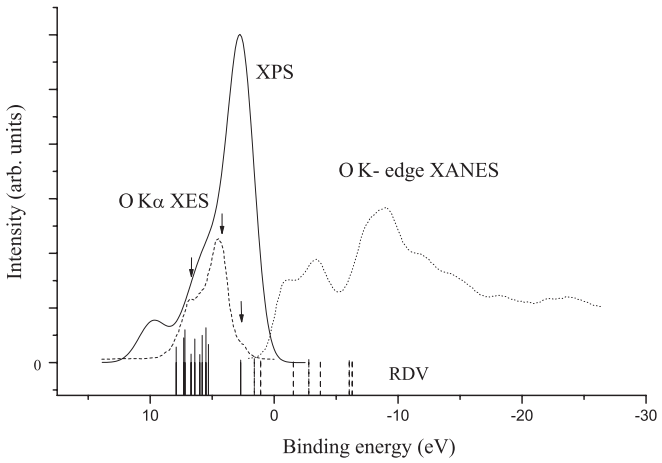

FIG. 11. Outer valence electrons XPS from PuO_2, O Kα x-ray emission spectrum [(O Kα XES; Ref. 53, x-ray absorption near O K-edge structure (XANES; Ref. 53)]. Vertical bars under the experimental spectra indicate the calculated densities of occupied (solid) and vacant (dash) O $2p$ states for PuO_2. The data are given with the background of one scale division below zero intensity. The spectra are reduced to the unified scale, where E_b(Pu $4f_{7/2}$) = 426.1 eV, E_b(Pu $5f$) = 2.6 eV, and E_b(O $1s$) = 530.1 eV. Spectral intensities were not normalized.

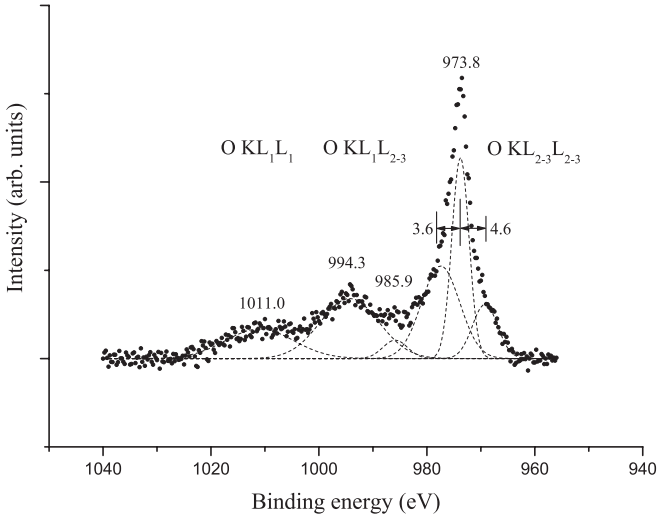

FIG. 12. O KLL Auger spectrum from PuO_2.

calculation results is qualitative, since the calculations were done for the ground state. Despite this, a qualitative agreement between the theory and the experiment was reached. Thus, the O Kα XES exhibits the two explicit peaks and a weak peak at 2.6 eV. The peak at 2.6 eV agrees with the fact that the $24\gamma_6^-$, $20\gamma_7^-$ OVMO consists mostly from the Pu $5f$ electronic states with a small admixture of the O $2p$ electronic states. Since the intensity of the peak at 2.6 eV ($24\gamma_6^-$, $20\gamma_7^-$ OVMO) is nine times lower than that of the peak at 4.9 eV (see the $23\gamma_6^-$–$21\gamma_6^+$ OVMO composition), one can evaluate the $24\gamma_6^-$, $20\gamma_7^-$ OVMO to contain 11% of the O $2p$ AO (Fig. 11). This value agrees with the corresponding calculated value equal to 14% (Table II). With this in mind, we can talk about the weakly bound localized (quasiatomic or quasicore) Pu $5f$ electrons ($24\gamma_6^-$, $20\gamma_7^-$ OVMO) and the delocalized bound Pu $5f$ electrons ($22\gamma_6^-$–$12\gamma_7^-$ MO).

The peak at 9.8 eV on the higher BE side from the basic OVMO XPS cannot be explained on the basis of the calculation results and the O K_α XES (Fig. 11). It confirms the fact that this peak cannot be attributed to the O $2p$ states; it appears, as it was noticed, due to the many-body perturbation during the photoemission of the quasiatomic Pu $5f$ electrons (shake-up satellite). Unfortunately, the emission spectrum structure does not allow an evaluation of the O $2p$ electron participation degree in the IVMO formation since this spectrum was measured in the restricted energy range. This energy range does not yield the IVMO $\rightarrow$ O $1s$ emission transition, whose spectrum should be observed in the energy range of 17.9–30.6 eV (Table III; Figs. 9–11).

The O $1s$ x ray absorption near-edge structure (O $1s$ XANES) agrees qualitatively with the calculation results for the ground state of the PuO_8 cluster (Fig. 11). Thus, if one shifts the calculation results to the right by $\sim$2 eV BE, the basic features of the triple-humped structure of the absorption edge will agree qualitatively with the experimental results. The experiment[43] showed that PuO_2 is a so-called Mott-Hubbard insulator, i.e., the occupied and vacant bands of the Pu $5f$ electrons are separated by the 1.8 eV gap. This agrees with Fig. 11 if one suggests that the lower vacant $21\gamma_7^-$ OVMO includes both the O $2p$ and the Pu $5f$ electronic states (Table II). It justifies the $\sim$2 eV shift of the calculated vacant O $2p$ states regarding the absorption spectrum.

The MO scheme for PuO_2 (Fig. 10) was also used to explain qualitatively the O KLL Auger spectral structure of PuO_2. For example, the O KLL Auger spectrum of Al_2O_3 with poorly formed IVMO is known to consist of three well-observable, poorly structured $\sim$9-eV-wide peaks reflecting the O $KL_{2\text{-}3}L_{2\text{-}3}$ (O $1s \leftarrow$ O $2p$), the O $KL_1L_{2\text{-}3}$ (O $1s \leftarrow$ O $2s$, $2p$), and the O KL_1L_1 (O $1s \leftarrow$ O $2s$) transitions.[70] The relative intensities of these O KLL Auger peaks are given as the O KLL Auger to the O $1s$ XPS intensity ratios. These relative intensities are important fundamental values. They allow a quantitative comparison of, for example, the O $2p$ partial DOS on oxygen ions in various oxides.[70]

The O $KL_{2\text{-}3}L_{2\text{-}3}$ (O $1s \leftarrow$ O $2p$) (Γ = 4.5 eV) Auger spectrum of PuO_2 reflects the filled O $2p$ DOS in PuO_2 (Fig. 12). The O $KL_{2\text{-}3}L_{2\text{-}3}$ FWHM agrees with the FWHM sums of the XPS O $1s$ electron peak (Γ = 1.1 eV, Fig. 2) and the O Kα XES ($\Gamma \sim 3$, Fig. 11) peak. This Auger line consists of the three peaks (see Fig. 12). The energy differences among these peaks agree satisfactorily with the corresponding energy differences among the three O Kα-emission peaks (see Fig. 11). The O $KL_1L_{2\text{-}3}$ (O $1s \leftarrow$ O $2s$, $2p$) peak reflects both the O $2p$ and the O $2s$ DOS. This peak is complicated and difficult to explain. The O KL_1L_1 (O $1s \leftarrow$ O $2s$) peak, reflecting mostly the DOS of the O $2s$ electrons participating in the IVMO formation in PuO_2, is highly structured. The FWHM of this peak, $\Gamma \sim 13$ eV, is comparable to that of the IVMO electrons in the XPS spectrum. It qualitatively confirms the participation of the O $2s$ electrons in the IVMO formation (Figs. 9–12). These results agree with the O KLL Auger data for UO_2 (Ref. 70).

In the conclusion, we would like to note that this paper studied the XPS structure of PuO_2 in the BE range of

0 eV–∼35 eV and established a correlation between the structure (OVMO- and IVMO-related) parameters with the participation of the Pu $6s$, $6p$, $5f$, $6d$, $7s$, $7p$, and the O $2s$, $2p$ electrons in the chemical bond formation.

V. CONCLUSIONS

The XPS of PuO_2 in the BE range of 0 eV–1250 eV were measured. The mechanisms of the spectral structure formation were considered. The quantitative interpretation of the XPS structure of the OVMOs (0 eV–∼15 eV BE) and the IVMOs (∼15 eV–∼35 eV BE) for plutonium dioxide, PuO_2, was done using the results of the RDV calculations of the finite clusters. The Pu $5f$ (1.82 Pu $5f$ e^-) electrons were theoretically shown and experimentally confirmed to participate directly in the chemical bond formation in PuO_2, slightly losing their f nature. They were shown to be delocalized within the outer valence band. The other part of the weakly bonded Pu $5f$ electrons (3.44 Pu $5f$ e^-) were shown to be localized at 2.6 eV. These results agree with the earlier photoelectron and x-ray emission spectroscopy data. The Pu $6p$ electrons, in addition to the effective (experimentally measurable) participation in the IVMO formation, were found to contribute noticeably (0.24 Pu $6p$ e^-) to the formation of the occupied part of the OVMO in PuO_2. The results of our investigation showed that the great role in the IVMO formation in PuO_2 was played by the Pu $6p_{3/2}$ and the O $2s$ AOs of the neighboring plutonium and oxygen ions. The MO sequent order in the BE range of 0 eV–∼35 eV for PuO_2 was defined, and the corresponding MO composition was obtained in the cluster calculations. With the BE differences between the core and valence electronic shells and the relativistic calculation results in mind, a quantitative MO scheme for PuO_2 was built. This MO scheme could be useful for understanding the nature of interatomic bonding in PuO_2 and for the interpretation of structures of other x-ray spectra of PuO_2.

ACKNOWLEDGMENT

This work was supported by RFBR Grant No. 13-03-00214.

*teterin_ya@nrcki.ru
†nonvitas@yandex.ru

[1] J. R. Naegele, J. Ghijsen, and L. Manes, Struct. Bonding **59-60**, 197 (1985).
[2] K. T. Moor and G. van der Laan, Rev. Mod. Phys. **81**, 235 (2009).
[3] D. Wang, W. F. van Gunstren, and Z. Chain, Chem. Soc. Rev. **41**, 5836 (2012).
[4] J. R. Naegele, L. Manes, J. C. Spirlet, and W. Muller, Phys. Rev. Lett. **52**, 1834 (1984).
[5] T. Almeida, L. E. Cox, J. W. Ward, and J. R. Naegele, Surf. Sci. **287-288**, 141 (1993).
[6] M. T. Butterfield, T. Durakiewicz, E. Guziewicz, J. J. Joyce, A. J. Arko, K. S. Graham, D. P. Moore, and L. A. Morales, Surf. Sci. **571**, 74 (2004).
[7] T. Gouder, A. Seibert, L. Havela, and J. Rebizant, Surf. Sci. **601**, L77 (2007).
[8] J. G. Tobin, D. A. Arena, B. Chung, P. Roussel, J. Terry, R. K. Schulze, J. D. Farr, T. Zocco, K. Heinzelman, E. Rotenberg, and D. K. Shuh, J. Nucl. Sci. Technol., Suppl. **3**, 98 (2002).
[9] S. W. Yu, J. G. Tobin, and P. Söderlind, J. Phys.: Condens. Matter **20**, 422202 (2008).
[10] R. Baptist, D. Courteix, J. Chayrouse, and L. Heintz, J. Phys. Ser. F **12**, 2103 (1982).
[11] L. E. Cox, Phys. Rev. B **37**, 8480 (1988).
[12] L. E. Cox and J. W. Ward, Inorg. Nucl. Chem. Lett. **17**, 265 (1981).
[13] L. Havela, T. Gouder, F. Wastin, and J. Rebizant, Phys. Rev. B **65**, 235118 (2002).
[14] K. T. Moore, M. A. Wall, A. J. Schwartz, B. W. Chung, D. K. Shuh, R. K. Schulze, and J. G. Tobin, Phys. Rev. Lett. **90**, 196404 (2003).
[15] N. Baclet, M. Dormeval, L. Havela, J. M. Fournier, C. Valot, F. Wastin, T. Gouder, E. Colineau, C. T. Walker, S. Bremier, C. Apostolidis, and G. H. Lander, Phys. Rev. B **75**, 035101 (2007).
[16] T. Gouder and L. Havela, J. Alloys Compd. **444-445**, 149 (2007).
[17] J. M. Wills, O. Eriksson, A. Delin, P. H. Andersson, J. J. Joyce, T. Durakiewicz, M. T. Butterfield, A. J. Arko, D. P. Moore, and L. A. Morales, J. Electron Spectrosc. Relat. Phenom. **135**, 163 (2004).
[18] M. T. Butterfield, K. T. Moore, G. van der Laan, M. A. Wall, and R. G. Haire, Phys Rev. B **77**, 113109 (2008).
[19] Y. A. Teterin, A. Y. Teterin, N. G. Yakovlev, I. O. Utkin, K. E. Ivanov, L. D. Shustov, L. D. Vukcevic, and G. N. Bek-Uzarov, Nuclear Technology & Radiation Protection **18**, 31 (2003).
[20] B. W. Veal, H. Diamond, and H. R. Hoekstra, Phys. Rev. B **15**, 2929 (1977).
[21] B. W. Veal, D. J. Lam, and H. Diamond, Physica B + C **86-88**, 1193 (1977).
[22] D. Courteix, J. Chayrouse, L. Heintz, and R. Baptist, Solid State Commun. **39**, 209 (1981).
[23] J. D. Farr, R. K. Schulze, and M. P. Neu, J. Nucl. Mater. **328**, 124 (2004).
[24] T. Bjorkman, O. Eriksson, and P. Andersson, Phys. Rev. B **78**, 245101 (2008).
[25] D. T. Larson, J. Vac. Sci. Technol. **17**, 55 (1980).
[26] H. G. Garcia Flores, P. Roussel, D. P. Moore, and D. L. Pugmire, Surf. Sci. **605**, 314 (2011).
[27] H. G. Garcia Flores and D. L. Pigmire, IOP Conf. Series: Mater. Sci. & Eng. **9**, 012038 (2010).
[28] H. Shi, M. Chu, and P. Zhang, J. Nucl. Mater. **400**, 151 (2010).
[29] J. G. Tobin, B. W. Chung, R. K. Schulze, J. Terry, J. D. Farr, D. K. Shuh, K. Heinzelman, E. Rotenberg, G. D. Waddill, and G. van der Laan, Phys. Rev. B **68**, 155109 (2003).
[30] J. Terry, R. K. Schulze, J. D. Farr, T. Zocco, K. Heinzelman, E. Rotenberg, D. K. Shuh, G. Van der Laan, D. A. Arena, and J. G. Tobin, Surf. Sci. **499**, L141 (2002).
[31] Y. A. Teterin and S. G. Gagarin, Russian Chemical Reviews **65**, 825 (1996).
[32] Y. A. Teterin and A. Y. Teterin, Russian Chemical Reviews **71**, 347 (2002).
[33] Y. A. Teterin and A. Y. Teterin, Russian Chemical Reviews **73**, 541 (2004).
[34] V. A. Gubanov, A. Rosen, and D. E. Ellis, J. Phys. Chem. Solids. **40**, 17 (1979).

[35]P. Zhang, B.-T. Wang, and X.-G. Zhao, Phys. Rev. B **82**, 144110 (2010).
[36]I. D. Prodan, G. E. Scuseria, and R. L. Martin, Phys. Rev. B **76**, 033101 (2007).
[37]D. A. Andersson, J. Lezama, B. P. Uberuaga, C. Deo, and S. D. Conradson, Phys. Rev. B **79**, 024110 (2009).
[38]L. Petit, A. Svane, Z. Szotek, W. M. Temmerman, and G. M. Stocks, Phys. Rev. B **81**, 045108 (2010).
[39]X. Wu and A. K. Ray, Physica B **301**, 359 (2001).
[40]X. Wu and A. K. Ray, Eur. Phys. J. B **19**, 345 (2001).
[41]J. C. Boettger and A. K. Ray, Int. J. Quantum Chem. **90**, 1470 (2002).
[42]I. D. Prodan, G. E. Scuseria, and R. L. Martin, Phys. Rev. B **73**, 045104 (2006).
[43]G. Jomard, B. Amadon, F. Bottin, and M. Torrent, Phys. Rev. B **78**, 075125 (2008).
[44]B. Sun, P. Zhang, and X.-G. Zhao, J. Chem. Phys. **128**, 084705 (2008).
[45]G. Jomard and F. Bottin, Phys. Rev. B **84**, 195469 (2011).
[46]Z. Rak, R. C. Ewing, and U. Becker, Surf. Sci. **608**, 180 (2013).
[47]A. Y. Teterin, M. V. Ryzhkov, Y. A. Teterin, L. Vukcevic, V. A. Terekhov, K. I. Maslakov, and K. E. Ivanov, Nuclear Technology & Radiation Protection **23**, 34 (2008).
[48]Y. A. Teterin and A. Y. Teterin, Nuclear Technology & Radiation Protection **19**, 3 (2004).
[49]A. Y. Teterin, M. V. Ryzhkov, Y. A. Teterin, L. Vukčević, V. A. Terekhov, K. I. Maslakov, and K. E. Ivanov, Radiochemistry **51**, 551 (2009).
[50]A. Y. Teterin, Y. A. Teterin, K. I. Maslakov, A. D. Panov, M. V. Ryzhkov, and L. Vukcevic, Phys. Rev. B **74**, 045101 (2006).
[51]I. O. Utkin, Y. A. Teterin, V. A. Terekhov, M. V. Ryzhkov, A. Y. Teterin, and L. Vukchevich, Radiochemistry **47**, 334 (2005).
[52]Y. A. Teterin, M. V. Ryzhkov, A. Y. Teterin, A. D. Panov, A. S. Nikitin, K. E. Ivanov, and I. O. Utkin, Nuclear Technology & Radiation Protection **17**, 3 (2002).
[53]A. Modin, Y. Yun, M.-T. Suzuki, J. Vegelius, L. Werme, J. Nordgren, P. M. Oppeneer, and S. M. Butorin, Phys. Rev. B **83**, 075113 (2011).
[54]D. A. Shirley, Phys. Rev. B **5**, 4709 (1972).
[55]T. Gouder and L. Havela, Mikrochim. Acta **138**, 207 (2002).
[56]P. Morrall, P. Roussel, L. Jolly, A. Brevet, and F. Delaunay, J. Nucl. Mater. **385**, 15 (2009).
[57]T. D. Chikalla, C. E. McHeilly, and R. E. Skavdahl, J. Nucl. Mater. **12**, 131 (1964).
[58]M. V. Ryzhkov, N. I. Medvedeva, and V. A. Gubanov, J. Phys. Chem. Solids **56**, 1231 (1995).
[59]A. Rosen and D. E. Ellis, J. Chem. Phys. **62**, 3039 (1975).
[60]D. E. Ellis and G. L. Goodman, Int. J. Quant. Chem. **25**, 185 (1984).
[61]O. Gunnarsson and B. I. Lundqvist, Phys. Rev. B **13**, 4274 (1976).
[62]P. Pyykko and H. Toivonen, Acta Acad. Aboensis, Ser. B **43**, 1 (1983).
[63]D. A. Varshalovish, A. N. Moskalev, and V. K. Khersonskii, *Quantum Theory of Angular Momentum* (World Scientific, Singapore, 1988).
[64]K. N. Huang, M. Aojogi, M. N. Chen, B. Graseman, and H. Mark, At. Data Nucl. Data Tables **18**, 243 (1976).
[65]M. Band, Y. I. Kharitonov, and M. B. Trzhaskovskaya, At. Data Nucl. Data Tables **23**, 443 (1979).
[66]V. G. Yarzhemsky, A. Y. Teterin, Y. A. Teterin, and M. B. Trzhaskovskaya, Nuclear Technology & Radiation Protection **27**, 103 (2012).
[67]J. C. Slater and K. H. Johnson, Phys. Rev. B **5**, 844 (1972).
[68]Y. A. Teterin, A. Y. Teterin, K. E. Ivanov, and I. O. Utkin, J. Nucl. Sci. Technol., Suppl. **3**, 140 (2002).
[69]A. Y. Teterin, M. V. Ryzhkov, Y. A. Teterin, K. I. Maslakov, T. Reich, and S. L. Molodtsov, Radiochemistry **51**, 560 (2009).
[70]Y. A. Teterin, K. E. Ivanov, A. Y. Teterin, A. M. Lebedev, I. O. Utkin, and L Vukchevich, J. Electron Spectrosc. Relat. Phenom. **101-103**, 401 (1999).